Electronic Supplementary Material (ESI) for Environmental Science: Nano.

# Supporting Information

| | |
|---|---|
| Authors | Dilpreet Singh, Georgios A. Sotiriou, Fang Zhang, Joey Mead, Dhimiter Bello, Wendel Wohlleben and Philip Demokritou |
| Title | End-of-life thermal decomposition of nano-enabled polymers: Effect of nanofiller-loading and polymer matrix on byproducts |
| Number of Pages | 16 |
| Number of Tables | 2 |
| Number of Figures | 6 |

## MATERIALS AND METHODS

### *Integrated Exposure Generation System (INEXS)*

Figure S1 shows the schematic of INEXS[1] used here to perform a systematic investigation of the thermal decomposition of NEPs under controlled combustion conditions. The platform enables thermal decomposition of an NEP, post-release treatment of the released aerosol through one of the three possible routes, and the detailed physicochemical, morphological and toxicological characterization of the byproducts, both in situ and ex situ. Briefly, a specified amount of the NEP (typically, 100 mg) is placed in a quartz crucible in the tube furnace and heated to a final temperature of 500 or 800 $^0$C over 40 mins. The released aerosol is then directed to one of the three possible post-release treatment scenarios. Route 1 is the 'no-treatment' scenario whereby the released aerosol is monitored and characterized as-is. In Route 2, the released aerosol undergoes treatment through a thermal denuder where the aerosol is heated to a temperature of 300 $^0$C to volatilize the semi-volatile organic compounds (sVOCs) which are then stripped off by an activated carbon section. The purpose of removing sVOCs from the released aerosol is to understand how the presence of sVOCs would impact the toxicology of released LCPM. Route 3 includes additional heat treatment of the released aerosol at a high temperature (800 $^0$C) for a minimum of 5 s of residence time, which is a requirement in commercial waste incinerators.[2] This treatment scenario enables a simulation of what would happen to the released LCPM upon further thermal processing. After undergoing one of the three possible post-release treatment scenarios, the aerosol is monitored for its size, concentration and gaseous composition using a variety of real-time instrumentation. Also, the released aerosol is size-fractionated and collected in the Harvard Compact Cascade Impactor[3–6], which can then be analyzed ex-situ.[7] The released aerosol may also be directed to an inhalation chamber for in-vivo toxicological characterization or in-vitro studies may be performed on the collected LCPM. The residual ash remaining in the crucible may also be recovered for detailed physicochemical and morphological characterization. High-Efficiency Particulate Air (HEPA) filtered ambient air is supplied at 5 L/min through the furnace during the entire thermal decomposition to support the oxygen requirement for incineration, maintaining the combustion atmosphere at ambient $N_2$:$O_2$ level.

### *Thermal decomposition scenarios*

In this study, all NEPs were investigated at two scenarios, corresponding to final thermal decomposition temperatures, $T_d$ = 500 and 800 $^0$C. The heating rates of the furnace corresponding to these final temperatures were 11.9 $^0$C/min and 19.4 $^0$C/min respectively based on 40 mins of ramping time from ambient (25 $^0$C) to the final temperature. The released aerosol was passed through Route 1 (no additional thermal treatment) for both scenarios. Route 1 was used for this study because the goal was to understand the nanofiller-loading and matrix effects on LCPM release and properties and not the effect of extended heat treatment or sVOC removal. Except for PC-based nanocomposites, 100 mg of each material was used for thermal decomposition. The amount used for PC-CNT was 35 mg, because higher amounts resulted in excessive particle generation and blockage of the Teflon filter (used as a substrate for particle sampling), causing a reduced flow of ambient air into the furnace and changing the combustion conditions.

### *Concentration and size of released aerosol*

The particle concentration and size of the released aerosol in the nano-regime (7.9-322 nm) were monitored in real time using a Scanning Mobility Particle Sizer (SMPS) Spectrometer (TSI Inc., Shoreview, MN). A sheath flow rate of 3 L/min and an aerosol flow rate of 0.3 L/min were used. Before passing through the SMPS, the released aerosol was diluted by a factor of 100 using the Rotating Disk Thermodiluter (TSI Inc., Shoreview, MN) to bring down the high particle concentration down to a measurable range for the SMPS. Particle concentration and size in the submicron and micron regime (0.5-20 μm) were also monitored in real time using the Aerodynamic Particle Sizer (APS) Spectrometer (TSI Inc., Shoreview, MN) in conjunction with the Aerosol Diluter (TSI Inc., Shoreview, MN) to dilute the released aerosol by a factor of 100. The particle concentration and size distribution presented in the results are as measured by the SMPS, and not adjusted for the dilution factor.

### *Collection, size-fractionation and gravimetric analysis of released aerosol*

The released aerosol was size-fractionated using the Harvard Compact Cascade Impactor (HCCI).[3] A flow of 30 L/min was used through the impactor to achieve the fractionation into three size-fractions, namely, $PM_{0.1}$, $PM_{0.1-2.5}$, and $PM_{>2.5}$. Polyurethane foam (PUF) substrates were used for collection of particles in the $PM_{0.1-2.5}$, and $PM_{>2.5}$ size fractions, whereas $PM_{0.1}$ particles were collected on either Teflon filters (Teflo Membrane, 47 mm diameter, 2 µm pore, Pall Corporation, Port Washington, NY) or quartz filters (Tissuquartz, 47 mm diameter, Pall Corporation, Port Washington, NY) depending on the required ex-situ analysis. All substrates and filters were chemically cleaned to remove any background contamination of trace metals and organics prior to particle sampling using a previously described protocol[4]. Gravimetric analysis was performed on each size fraction by subtracting the pre-collection weight from the post-collection weight of the substrate or filter after conditioning them at a controlled temperature of 70 $^0$F (21 $^0$C or 294 K) and relative humdity of 30-35% for at least 48 hours utilizing a Mettler-Toledo XPE analytical microbalance (Columbus, OH).

### *Chemical characterization of released aerosol and residual ash*

Both the released aerosol and residual ash were characterized in terms of their elemental/organic carbon content and elemental composition. For EVA-$TiO_2$ nanocomposites, the element of interest in the released aerosol and residual ash was titanium (subsequently converted to equivalent $TiO_2$) in order to quantify how much of the nanofiller was released into the air and retained in the residual ash. For PP-CNT and PC-CNT, the element analyzed in the released aerosol and residual ash was aluminum because aluminum was present in the highest concentration among other metal catalysts used for manufacture of the CNTs used in this study[8] and hence could be used as a surrogate for detection of CNTs in the released aerosol and residual ash (assuming there was no change in Al concentration of CNT upon thermal decomposition).

Elemental and organic carbon content (EC-OC) of the residual ash and the $PM_{0.1}$ size fraction of the released aerosol was determined by gas chromatography/mass spectrometry (GC-MS). A 1 cm$^2$ filter punch on the quartz filter (containing the released aerosol) was used to measure EC-OC following the protocols standardized for the ACE-Asia intercomparison study[9]. This method is adapted from the NIOSH 5040 method, which utilizes the Sunset Laboratory Inc. laboratory-based thermal-optical analyzer.

Elemental analysis (Ti and Al) of the released aerosol ($PM_{0.1}$) and residual ash was performed by magnetic sector field inductively coupled plasma mass spectrometry (SF-ICPMS) following the published protocol[10]. The Teflon filter (containing the released aerosol) and the bulk residual ash were solubilized using a mixed acid (1 mL of 16M Nitric, 0.25 mL of 12M Hydrochloric, 0.1 mL of 28M Hydrofluoric), microwave-aided digestion in sealed Teflon vials. The digest solutions were diluted to 15 mL with high-purity water (Millipore) in acid-washed low-density polyethylene (LDPE) bottles. Finally, the digested samples and extracts underwent SF-ICPMS analysis (Thermo-Finnigan Element 2) for quantification of specific metals. In addition to the collected samples, the analytical batches included sample spikes, sample duplicates, method and instrument blanks, and certified reference materials (NIST 2709, NIST 1648a, NIST 2556, NIST 2702) for quality assurance.

### *Morphological characterization of released aerosol and residual ash*

Scanning electron microscopy (SEM, Zeiss Supra 55VP Field Emission Scanning Electron Microscope, Jena, Germany) was used to characterize the morphology of the released aerosol ($PM_{0.1}$) and residual ash samples. Particulate matter on the Teflon filter was extracted by placing the filter in 20 mL of pure ethanol followed by mild bath ultrasonication (Branson 1510 Ultrasonic Cleaner, Branson Ultrasonics, Danbury, CT) for 30 s. A drop of the suspension was placed on a pre-cleaned 5 mm x 5mm silicon wafer chip (Ted Pella, Redding, CA) that was mounted on a double-coated carbon conductive tape (Ted Pella, Redding, CA) placed on a pin stub mount (Ted Pella, Redding, CA). The suspension was then allowed to dry under ambient conditions. As for the residual ash, a small piece of the ash was directly placed on the carbon tape placed on the stub mount. The SEM was operated at 2-5 kV EHT (Extra High Tension) and both the secondary electron and in-lens detectors were employed.

## FIGURES AND TABLES

Figure S1 shows the schematic of INEXS[1] used here to perform a systematic investigation of the thermal decomposition of NEPs under controlled combustion conditions.

Figure S2 shows the released aerosol concentration evolution and mobility size distribution for EVA-, PP- and PC-based nanocomposites for $T_d$ = 500 $^0$C. Figure S2A shows that the particle evolution profile and the peak particle concentration differ between the various loadings of titania. The peak particle concentration for EVA-2% (~ 1.2 x $10^6$ #/cm$^3$) is greater by a factor of 1.7 than that for EVA-15% (~ 7.2 x $10^5$ #/cm$^3$). Furthermore, EVA-2% reaches the peak around 36 minutes (453 $^0$C) whereas EVA-15% peaks around 42 minutes (500 $^0$C). EVA has the highest mean mobility diameter (~ 126 nm), approximately 1.5 times higher than that of EVA-15% (~ 83 nm) (Figure S2C). The maximum particle concentration of PP-CNT (~ 5.6 x $10^5$ #/cm$^3$) is 6 times higher than that of PC-CNT (9.3 x $10^4$ #/cm$^3$) (Figure S2B). The mean mobility diameter of PP-CNT (182 nm) is comparable to that of PC-CNT (185 nm) (Fig. S2D).

Figure S3 shows the mass-size distributions of all the nanocomposites for $T_d$ = 500 and 800 $^0$C. For $T_d$ = 800 $^0$C, $PM_{0.1}$ accounts for most of the released aerosol (50-70 wt%), followed by $PM_{0.1-2.5}$ (30-45 wt%) and $PM_{>2.5}$ (< 5 wt%) irrespective of the titania loading (Figure S3A). PP-CNT and PC-CNT have distinctly different mass size distributions (Figure S3B). $PM_{0.1-2.5}$ dominates the released aerosol from PP-CNT (~ 60 wt%) followed by $PM_{0.1}$ (~ 38 wt%) and $PM_{>2.5}$ (< 3 wt%), unlike PP which has $PM_{0.1}$ as the greater fraction. $PM_{0.1}$ is the dominant size fraction for PC-CNT (55 wt%) followed by $PM_{0.1-2.5}$ (43 wt%) and $PM_{>2.5}$ (< 3 wt%), similar to PC. For $T_d$ = 500 $^0$C, $PM_{0.1}$ dominates the released aerosol (55-70 wt%) followed by $PM_{0.1-2.5}$ (25-40 wt%) and $PM_{>2.5}$ (< 5 wt%), irrespective of the loading of titania in the EVA matrix (Figure S3C). PP-CNT, PC and PC-CNT display similar distributions with $PM_{0.1}$ as the dominant fraction (> 55 wt%) followed by $PM_{0.1-2.5}$ (30-40 wt%) and $PM_{>2.5}$ (< 3 wt%) (Figure S3D). However, PP shows $PM_{0.1-2.5}$ as the dominant fraction.

Figure S4 shows the time evolution of carbon monoxide and oxygen concentrations in the tube furnace over the entire thermal decomposition duration for PC-CNT at $T_d$ = 800 $^0$C. The peak CO concentration

(~ 1700 ppm) and the lowest $O_2$ concentration (20.2 vol%) occur at the same time point (23 mins), indicating the peak of thermal decomposition. Since the oxygen concentration does not drop significantly below the ambient concentration (20.9 vol%), it indicates that the combustion occurs in sufficient oxygen conditions and assures complete combustion of the NEP.

Figure S5 shows the EC-OC distribution and elemental analysis of the released aerosol for all the nanocomposites for $T_d$ = 500 $^0$C. The released aerosol for all the titania loadings is dominated by organic carbon (> 99.6 wt%) (Figure S5A), as also for both PP-CNT and PC-CNT (> 99.2 wt%) (Figure S5B). The released titania concentration is highest for EVA-5% (~ 0.026 wt%), approximately 40 times higher than that for both EVA-2% and EVA-15% (Figure S5C). PP-CNT shows a released aluminum concentration of ~ 0.006 wt%, approximately 8 times higher than that for PC-CNT (~0.0008 wt%) (Figure S5D).

Figure S6 shows two XRD patterns of residual ashes from EVA-15% $TiO_2$ for $T_d$ = 500 and 800 $^0$C. The crystal phase at both temperatures is anatase, as identified by characteristic peaks around 25$^0$ and 48$^0$. Analysis of crystal size using Scherrer's formula reveals that the nanofiller size increases from 14.2 nm at $T_d$ = 500 $^0$C to 23.5 nm at $T_d$ = 800 $^0$C.

**Table S1.** Summary of the nano-enabled products used in this study, listing the host polymer matrix, the nanofiller type, size and loading, and the potential industrial applications of the polymer nanocomposites.

| Polymer | Nanofiller | Size (nm) | Loading (wt%) | Applications |
|---|---|---|---|---|
| Polypropylene (PP) | Multi-walled carbon nanotubes (CNT) | Diameter: 10 | 0, 3 | Packaging,[11,12] textiles,[13] lab equipment[14] and automotive parts[14] |
| Polycarbonate (PC) | Multi-walled carbon nanotubes (CNT) | Diameter: 10 | 0, 3 | Electronics, automobiles, food/drink containers and construction materials[15–17] |
| Ethylene-vinyl acetate (EVA) | $TiO_2$ | 7 | 0, 2, 5, 15 | Biomedical devices, sports equipment, adhesives and coatings[18,19] |

**Table S2.** Summary of the nano-enabled products used in this study, along with the yield (with respect to mass of NEP used) obtained for the released aerosol, residual ash and gaseous compounds upon thermal decomposition at $T_d$ = 500 and 800 $^0$C.

| Nano-enabled product (NEP) | | | Yield (wt%) | | | | | |
|---|---|---|---|---|---|---|---|---|
| | | | 500 $^0$C | | | 800 $^0$C | | |
| Sample ID | Nanofiller | Loading (wt%) | Released Aerosol | Residual Ash | Gaseous Release | Released Aerosol | Residual Ash | Gaseous Release |
| EVA | - | - | 7.4 | 0.0 | 92.6 | 8.4 | 0.0 | 91.6 |
| EVA | $TiO_2$ | 2 | 7.6 | 2.2 | 90.2 | 7.3 | 1.7 | 91.0 |
| EVA | $TiO_2$ | 5 | 7.1 | 4.9 | 88.0 | 7.7 | 4.3 | 88.0 |
| EVA | $TiO_2$ | 15 | 5.8 | 14.2 | 80.0 | 7.2 | 13.6 | 79.2 |
| PP | - | - | 23.6 | 0.0 | 76.4 | 39.3 | 0.0 | 60.7 |
| PP | CNT | 3 | 16.2 | 2.4 | 81.4 | 18.4 | 0.0 | 81.6 |
| PC | - | - | 3.7 | 32.0 | 64.3 | 11.5 | 0.0 | 88.5 |
| PC | CNT | 3 | 7.5 | 35.0 | 57.5 | 10.6 | 0.0 | 89.4 |

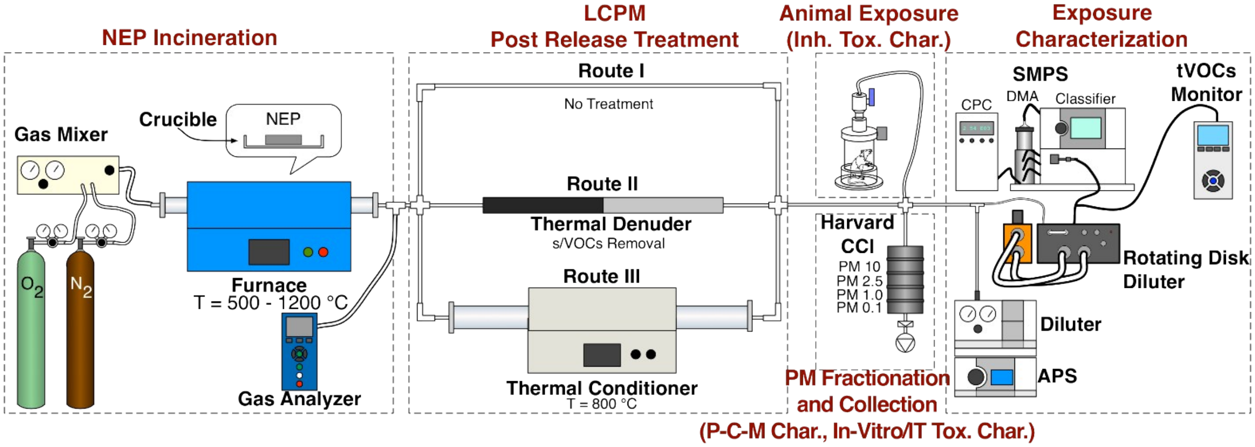

**Figure S1.** Schematic of the Integrated Exposure Generation System (INEXS) consisting of 3 modules, namely, the incineration of nano-enabled product under controlled conditions, the post-release aerosol treatment and the aerosol size-fractionated collection and exposure characterization (both in-situ and ex-situ).

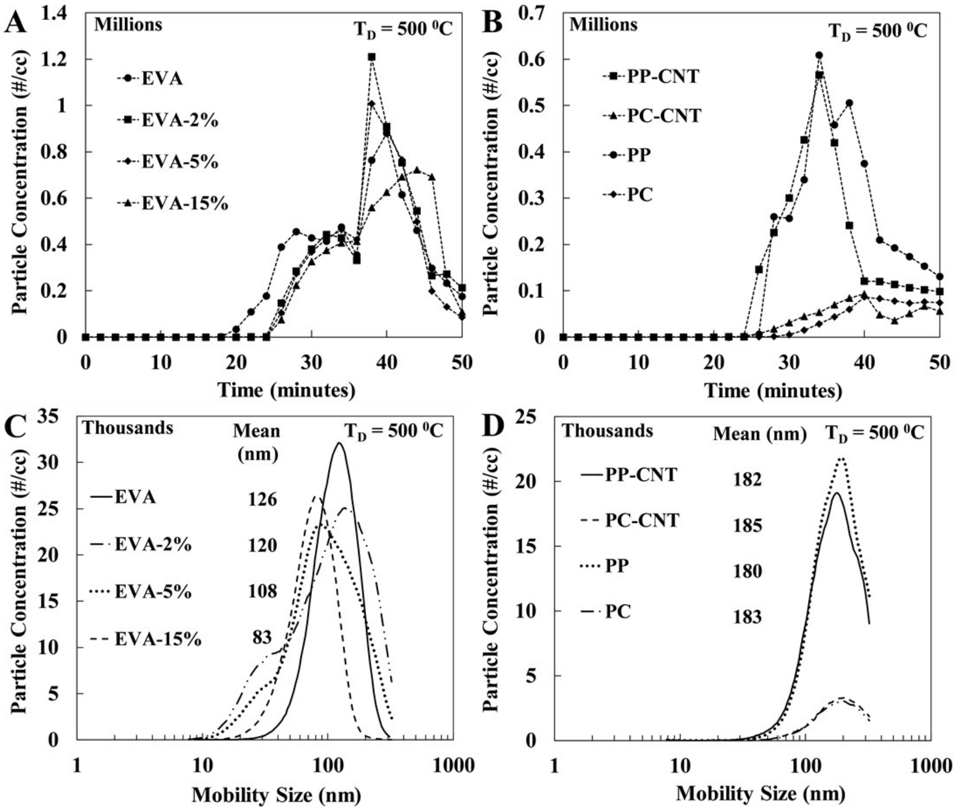

**Figure S2.** Released aerosol concentration and mobility size for final thermal decomposition temperature, $T_d$ = 500 $^0$C. The particle concentration over time and snapshot of the particle mobility size distribution at the time of maximum particle concentration for EVA-based nanocomposites at different titania loadings (0, 2, 5, 15 wt%) (A and C) and PP- and PC-based nanocomposites (3 wt% CNT loading each) (B and D).

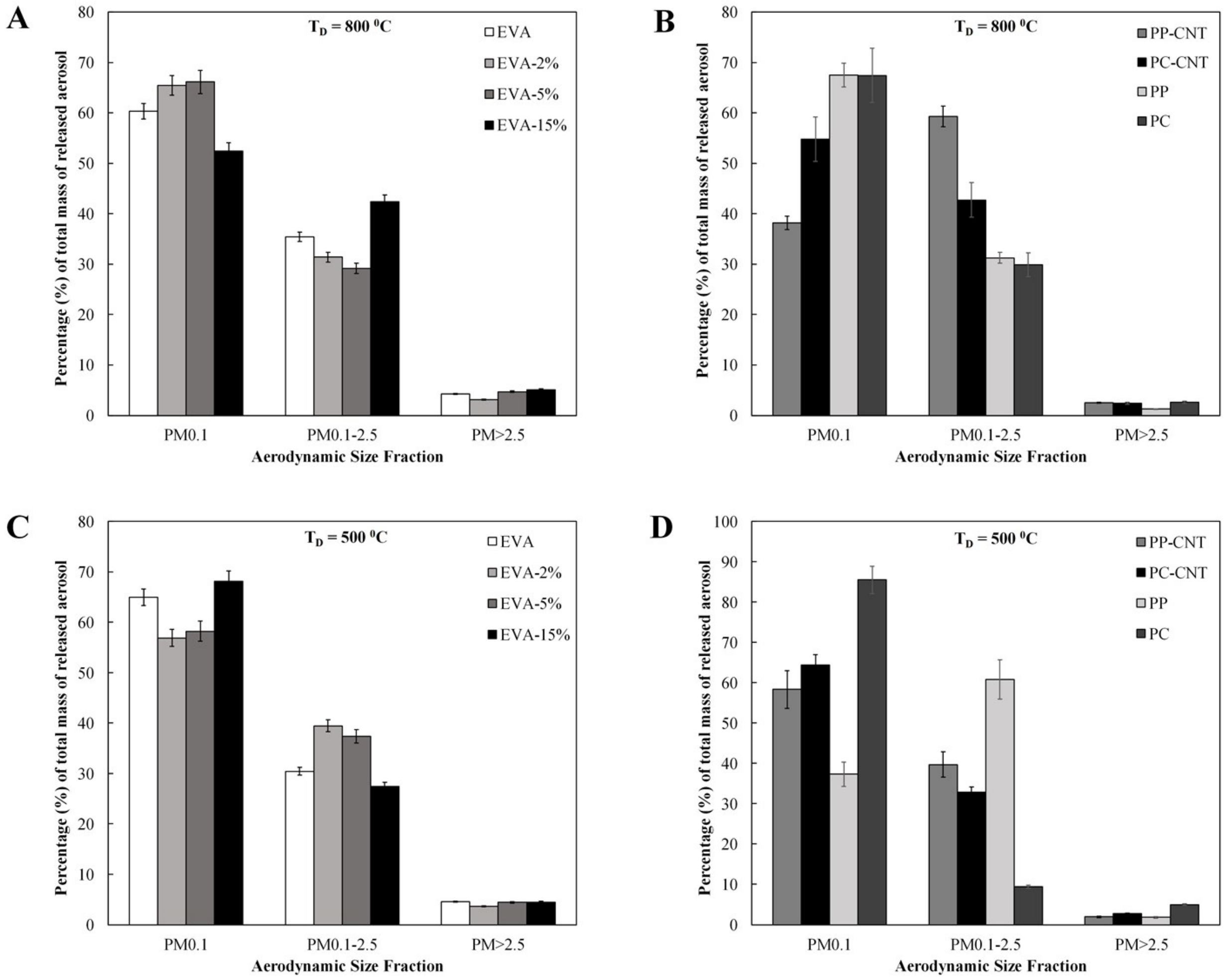

**Figure S3.** Mass-aerodynamic size distribution of the released aerosol for final thermal decomposition temperature, $T_d$ = 500 and 800 $^0$C. Fraction of mass of released particles collected in the 3 size fractions ($PM_{0.1}$, $PM_{0.1-2.5}$, $PM_{>2.5}$) for EVA-based nanocomposites at different titania loadings (0, 2, 5, 15 wt%) (A and C) and PP- and PC-based nanocomposites (3 wt% CNT loading each) (B and D), using size-fractionation by the Harvard Compact Cascade Impactor (HCCI).[3]

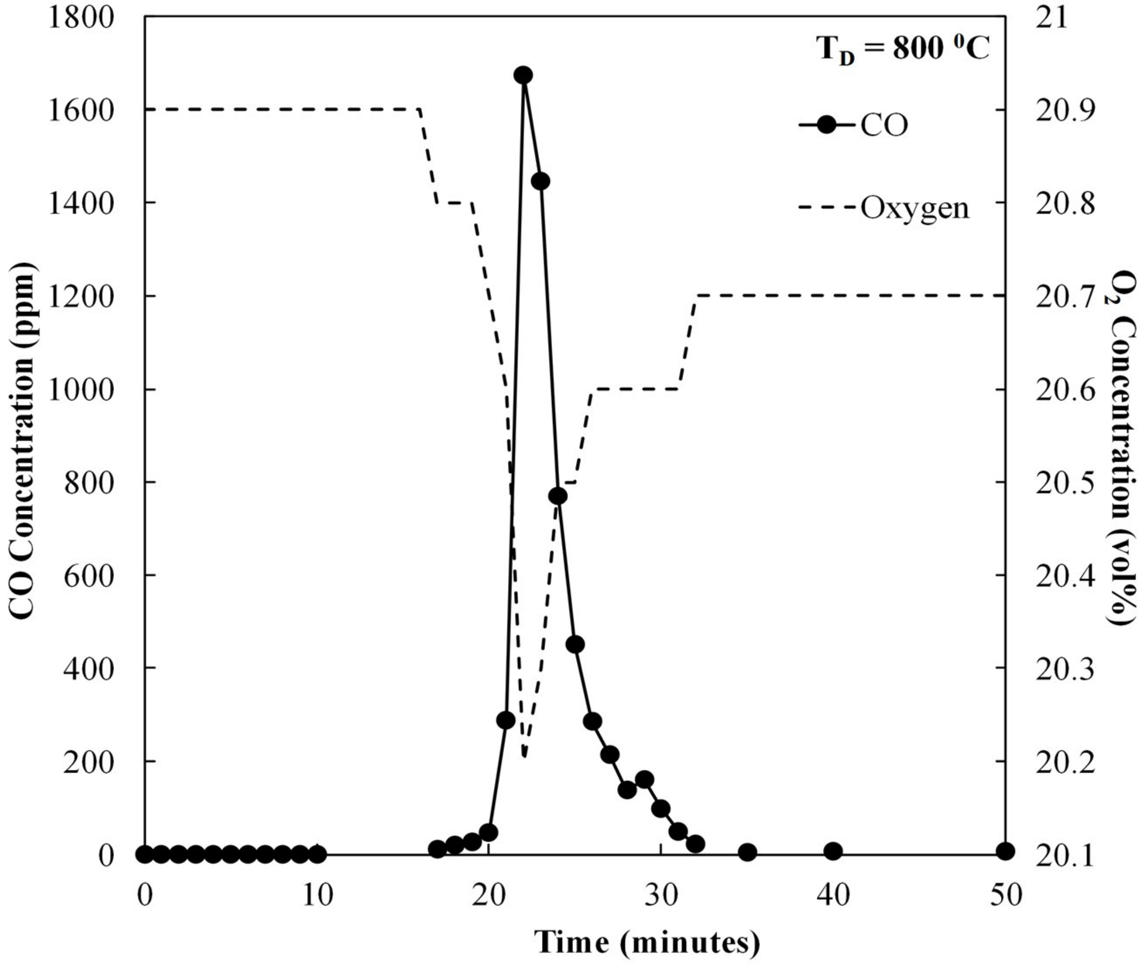

**Figure S4.** Time evolution of carbon monoxide (CO) and oxygen ($O_2$) concentrations in the off-gas for final thermal decomposition temperature, $T_d$ = 800 $^0$C, for PC-3% CNT.

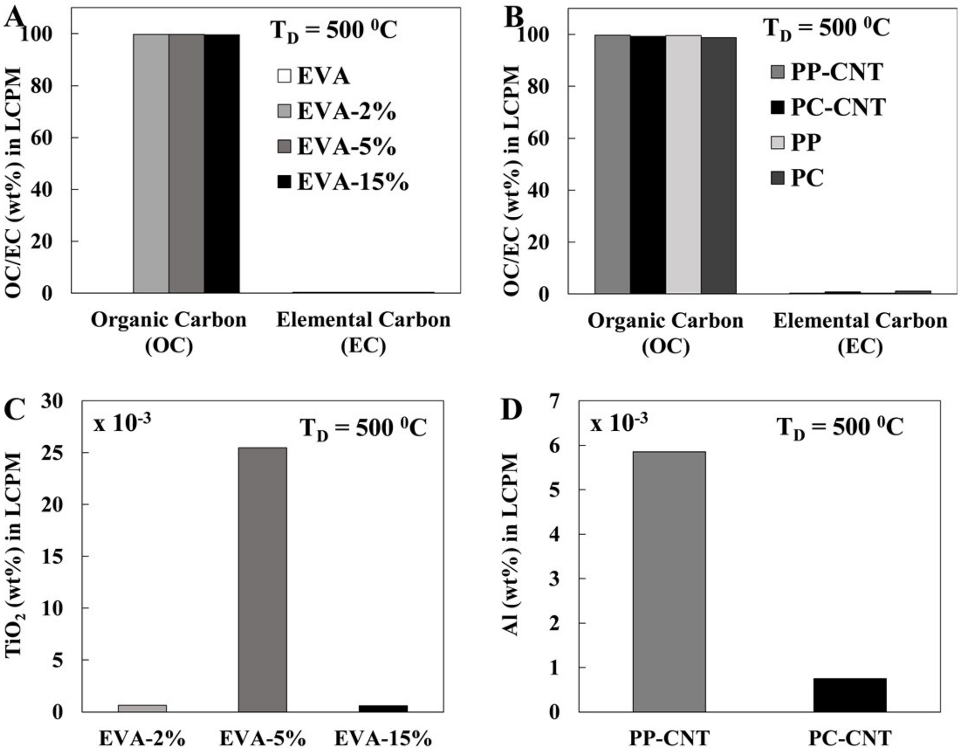

**Figure S5.** Elemental-organic carbon distribution and concentration of nanofiller-related metals in the released aerosol for final thermal decomposition temperature, $T_d$ = 500 $^0$C, for EVA-based nanocomposites at different titania loadings (0, 2, 5, 15 wt%) (A and C), and PP- and PC-based nanocomposites (3 wt% CNT loading each) (B and D).

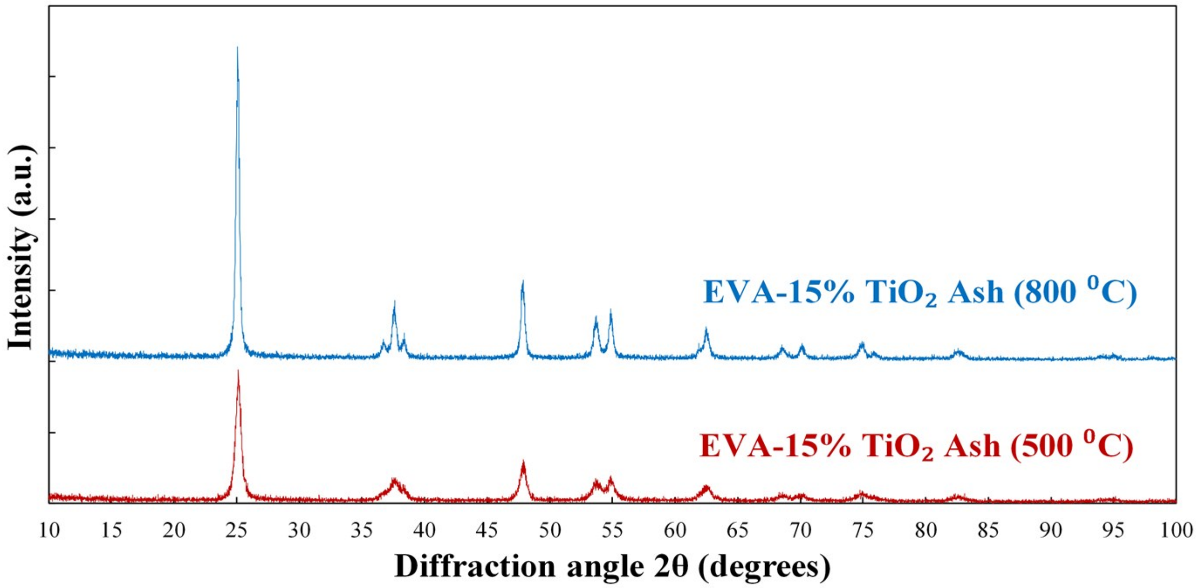

**Figure S6.** X-Ray Diffraction (XRD) patterns of residual ash from EVA-15% $TiO_2$ for final thermal decomposition temperature, $T_d$ = 500 $^0$C (red line) and 800 $^0$C (blue line).

# References

1 G. A. Sotiriou, D. Singh, F. Zhang, W. Wohlleben, M.-C. G. Chalbot, I. G. Kavouras and P. Demokritou, *Environ. Sci. Nano*, 2015, **2**, 262–272.

2 M. J. Clarke, M. de Kadt, D. Saphire and S. R. Golden, *Burning garbage in the US: practice vs. state of the art*, INFORM, 1991.

3 P. Demokritou, S. J. Lee, S. T. Ferguson and P. Koutrakis, *J. Aerosol Sci.*, 2004, **35**, 281–299.

4 D. Bello, J. Martin, C. Santeufemio, Q. Sun, K. Lee Bunker, M. Shafer and P. Demokritou, *Nanotoxicology*, 2012, **7**, 1–15.

5 S. V Pirela, G. Pyrgiotakis, D. Bello, T. Thomas, V. Castranova and P. Demokritou, *Inhal. Toxicol.*, 2014, **26**, 400–8.

6 C. Chang, P. Demokritou, M. Shafer and D. Christiani, *Environ. Sci. Process. Impacts*, 2013, **15**, 214–24.

7 A. K. Pal, C. Y. Watson, S. V. Pirela, D. Singh, M. C. G. Chalbot, I. Kavouras and P. Demokritou, *Toxicol. Sci.*, 2015, **146**, 321–333.

8 P. Boonruksa, D. Bello, J. Zhang, J. A. Isaacs, J. L. Mead and S. R. Woskie, *Ann. Occup. Hyg.*, 2015, mev073.

9 J. J. Schauer, B. T. Mader, J. T. Deminter, G. Heidemann, M. S. Bae, J. H. Seinfeld, R. C. Flagan, R. A. Cary, D. Smith, B. J. Huebert, T. Bertram, S. Howell, J. T. Kline, P. Quinn, T. Bates, B. Turpin, H. J. Lim, J. Z. Yu, H. Yang and M. D. Keywood, *Environ. Sci. Technol.*, 2003, **37**, 993–1001.

10 J. D. Herner, P. G. Green and M. J. Kleeman, *Environ. Sci. Technol.*, 2006, **40**, 1925–1933.

11 S. Allahvaisi, in *Polypropylene*, ed. F. Dogan, InTech, Rijeka, 2012.

12 D. Bikiaris, *Materials (Basel).*, 2010, **3**, 2884–2946.

13 A. Marcinčin and M. Jambrich, Springer Netherlands, 1999, pp. 813–820.

14 H. A. Maddah and H. A. Maddah, *Am. J. Polym. Sci.*, 2016, **6**, 1–11.

15 Transparency Market Research, *Global Polycarbonate Market- Industry Analysis, Size, Share, Trends & Forecast 2014-2020*, Albany, 2015.

16 W. Zhang, J. Suhr and N. Koratkar, *J. Nanosci. Nanotechnol.*, 2006, **6**, 960–964.

17 S. Pande, A. Chaudhary, D. Patel, B. P. Singh and R. B. Mathur, *RSC Adv.*, 2014, **4**, 13839–13849.

18 A. M. Henderson, *IEEE Electr. Insul. Mag.*, 1993, **9**, 30–38.

19 J. Gonzalez-Benito, E. Castillo and J. F. Caldito, *Eur. Polym. J.*, 2013, **49**, 1747–1752.